Motif structure for the four subgroups within the suprachiasmatic nuclei affects its entrainment ability

Zheng, W.X.; Gu, C.G.; Yang, H.J.; Rohling, J.H.T.

Motif structure for the four subgroups within the suprachiasmatic nuclei affects its entrainment ability

Wenxin Zheng,[1] Changgui Gu,[1,2,*] Huijie Yang,[1] and Jos H. T. Rohling[2,†]

[1]*Business School, University of Shanghai for Science and Technology, Shanghai 200093, People's Republic of China*

[2]*Department of Molecular Cell Biology, Laboratory for Neurophysiology, Leiden University Medical Center, Leiden 2300RC, The Netherlands*

(Received 5 September 2021; revised 13 December 2021; accepted 12 January 2022; published 27 January 2022)

Circadian rhythms of physiological and behavioral activities are regulated by a central clock. This clock is located in the bilaterally symmetrical suprachiasmatic nucleus (SCN) of mammals. Each nucleus contains a light-sensitive group of neurons, named the ventrolateral (VL) part, with the rest of the neurons being insensitive to light, named the dorsomedial (DM) group. While the coupling between the VL and DM subgroups have been investigated quite well, the communication among the four subgroups across the nuclei did not get a lot of attention. In this article, we theoretically analyzed seven motiflike connection patterns to investigate the network of the two nuclei of the SCN as a whole in relation to the function of the SCN. We investigated the entrainment ability of the SCN and found that the entrainment range is larger in the motifs containing a link between the two VL parts across the nuclei, but it is smaller in the motifs that contain a link between the two DM parts across the nuclei. The SCN may strengthen or weaken connections between the left and right nucleus to accomodate changes in external conditions, such as resynchronization after a jet lag, adjustment to photoperiod or for the aging SCN.

DOI: 10.1103/PhysRevE.105.014314

I. INTRODUCTION

The environmental light-dark cycle of 24 h has profound consequences for our daily lives. Our physiology is fully adapted to this rhythmic environment, as are those of most organisms on earth [1–3]. Going against these rhythms can be detrimental for health. In mammals, the suprachiasmatic nucleus (SCN) [4–8] is a master clock that regulates these 24 h (circadian) rhythms. The SCN is a bilaterally symmetric structure above the optic chiasm, with a nucleus left and right of the third ventricle. Each nucleus is composed of approximately 10 000 neurons that are generally divided into a light-sensitive subgroup of neurons, often associated with the ventrolateral (VL) part of the SCN, and a light-insensitive subgroup of neurons, associated with the dorsomedial (DM) part of the SCN. These subgroups are interconnected through different neurotransmitters and form a neuronal network [9–13].

Interestingly, experimental research showed that the circadian rhythms remain even in the absence of a light-dark cycle. Since, there has been a lot of research done to understand how the rhythmic behaviors emerge at different levels. At the level of single cells, the rhythm originates from the a genetic negative feedback loop [13–16]. At the level of the whole SCN network, these robust single cell rhythms must be synchronized to create a robust circadian output rhythm [15].

In normal circumstances, the near-24 h endogenous rhythms are entrained to the external light-dark cycle. However, disturbances in these external lighting conditions can disturb these rhythms, for example, intercontinental flights can cause a jet lag, or artificial light at night may cause disturbances. The rhythm must be flexible enough to be able to adjust to this sudden shift in light conditions after intercontinental flight. However, there must be a fine balance between flexibility of these rhythms and robustness of the rhythm, because we do not want a jet lag every time we switch on the light at a wrong time of the night [17]. In mammalian experimental research it was found that the synchronization between the VL and the DM plays a key role in the recovery from jet lag. During the recovery, the VL immediately shifts to the phase of new environment, but the DM synchronizes to the new phase only after several days [10,11,18]. When exposed to constant light conditions, the behavioral activity of mammals may exhibit two periodic components of 24 h that are in antiphase, where the phase difference between the two components is around 12 h. Further experiments revealed that the two antiphase components are regulated by the two nuclei of the SCN operating in antiphase [19]. This phenomenon is known as "splitting." Another phenomenon named "dissociation" can be explained by the desynchronization (uncoupling) between the VL and the DM within each nucleus. In detail, exposed to an artificial light-dark cycle of 22 h, the behavioral activity may exhibit two periodic components of which one has a period of 22 h and the other has a period of 24 h [20,21]. It was found that the 22 h component is controlled by the light-sensitive part, i.e., the VL, and the 24 h component is controlled by the light-insensitive part, i.e., the DM.

*gu_changgui@163.com
†J.H.T.Rohling@lumc.nl

To understand the mechanism for the balanced robust and flexible rhythms of the SCN, it is important to investigate the synchronization achieved through coupling within and between (sub)groups of the neurons [22,23]. Current experiments reveal that the cellular coupling is mainly through neurotransmitters that are different between the VL and the DM [18,24–26]. The most important neurotransmitter expressed in the VL is vasoactive intestinal polypeptide (VIP), while the DM neurons are mainly characterized by arginine vasopressin (AVP) [25,26]. The VL and the DM within one nucleus of the SCN synchronize their periods through coupling pathways containing γ-aminobutyric acid (GABA), which is very abundant and is expressed in most SCN neurons [18,26–28]. However, the precise coupling mechanisms are unclear between the right and the left nucleus [22], and further, how the four subgroups are coupled across the nuclei.

In most of the previous theoretical studies only the coupling in a single nucleus of the SCN was considered (e.g., Refs. [29–31]). In this paper, we want to take both nuclei into consideration, making use of network motifs. Motifs are frequently occurring subgraphs of networks, typically consisting of three or four nodes [32]. If a subgraph appears much more frequently than expected in random networks, then it is considered to be a motif. The network motif patterns have been described as the basic building blocks of network structure [32,33]. Previous studies identified motifs to be present in brain networks [34–36] and play important roles in brain network dynamics [37,38]. Other studies showed that motifs can give insight into the function of brain networks [39]. It has been suggested that statistical information of motifs can help in understanding the global function of the entire network. On the mesoscale level of healthy and abnormal brain networks, motifs had been considered to be an important feature [39–41]. Motifs have also been used to classify networks into superfamilies, with different motif fingerprints shaped by different functional roles [33]. Moreover, changes in the motif frequencies of so-called progression networks for patients suffering from Alzheimer's disease have been discovered [42], showing that motif analysis may provide potentially powerful new biomarkers.

In this paper, we study the motif structures to analyze the four-component network of the SCN. We use possible four-node motifs to study the function of the SCN network. Because the neuronal oscillators in the two subgroups of the SCN single nucleus are interrelated, and the left and the right nuclei of the SCN are symmetrical, we propose seven possible motifs. Although we cannot determine whether these motifs really constitute the SCN network, we can determine the motif that establishes the SCN function best. We will use the range of entrainment of the SCN as a measure. The entrainment range is an important property of the SCN which represents the flexibility of the SCN to adapt to changes in the environment. Mammals can be entrained to not only the natural 24 h light-dark cycle, but also light-dark cycles with artificial periods [2,3]. For example, for *Rattus morvegicus*, *Homo sapiens*, and *Arivicanthis niloticus*, the entrained artificial periods are from 23.5 (named lower limit of entrainment) to 28.5 h (named higher limit of entrainment), from 21.5 to 28.6 h, and from 22.5 to 25.5 h, respectively [2,20,43]. The range between the lower limit of entrainment (LLE) and the higher limit of entrainment is called entrainment range [44,45]. This makes this measure a good measure to investigate circadian clock function.

In the present work, we propose that there are seven possible motifs for the connections of the four subgroups and investigate the effect of the motif structure on one of the main functions of the SCN, the entrainment range, based on a Poincaré model [3,46–49]. The rest of this paper is organized as follows. In Sec. II, each motif structure is briefly described and the Poincaré model is introduced exposed to the external cycle. In Sec. III, the numerical results of the entrainment range are compared between motifs. After that, in Sec. IV, theoretical analysis is presented to confirm the simulation results in Sec. III. Finally, the conclusion and discussion are shown in Sec. V.

II. METHODS

A. Potential motifs

Thus far, it is evident that the VL and the DM are mutually coupled within each nucleus of the SCN and the two nuclei are symmetrical, but the details for the connection between the right nucleus and the left nucleus are unclear. Accordingly, as we assume that the two nuclei are symmetrical, we propose that there are seven potential motifs for the four subgroups. Figure 1 shows the structure of each motif, where one node represents one subgroup and one link represents the connection between two subgroups. For simplicity, we assume that the neurons within each subgroup are all-to-all connected, and if there is a connection between two subgroups in Fig. 1, all neurons within one subgroup connect with all neurons within another subgroup. Note that the direction of the link is not taken into account in the present study. In the following sections, VL_R and the DM_R represent the VL and the DM in the right nucleus of the SCN, respectively, and the VL_L and the DM_L represent the VL and the DM in the left nucleus of the SCN, respectively.

The topology of the SCN network is described by an adjacency matrix e: if there is a link between two nodes i and j, $e_{ij} = e_{ji} = 1$; and if no link exists between i and j, $e_{ij} = e_{ji} = 0$, $1 \leqslant i, j \leqslant N$, where N is the total number of the SCN neurons. For simplicity, we assume that the number of neurons is equal, i.e., $\frac{N}{4}$, for each subgroup without special statement.

B. Description of Poincaré model

Circadian neuronal oscillators are often described by the Goodwin model and the Poincaré model, both of which contain phase and amplitude information [50,51]. In the Goodwin model, a generic feedback loop constitutes an oscillator, and in the Poincaré model, the oscillator is based on a more general description. The Poincaré model is chosen in the present study, because of its generality and more straightforward way of performing theoretical analysis.

In this study, we consider the networked Poincaré model composed of N neuronal oscillators [52–54]. Each neuronal oscillator has two variables, x and y [3,46,48,55]. The dynamics of the i_{th} oscillator is governed by the following set

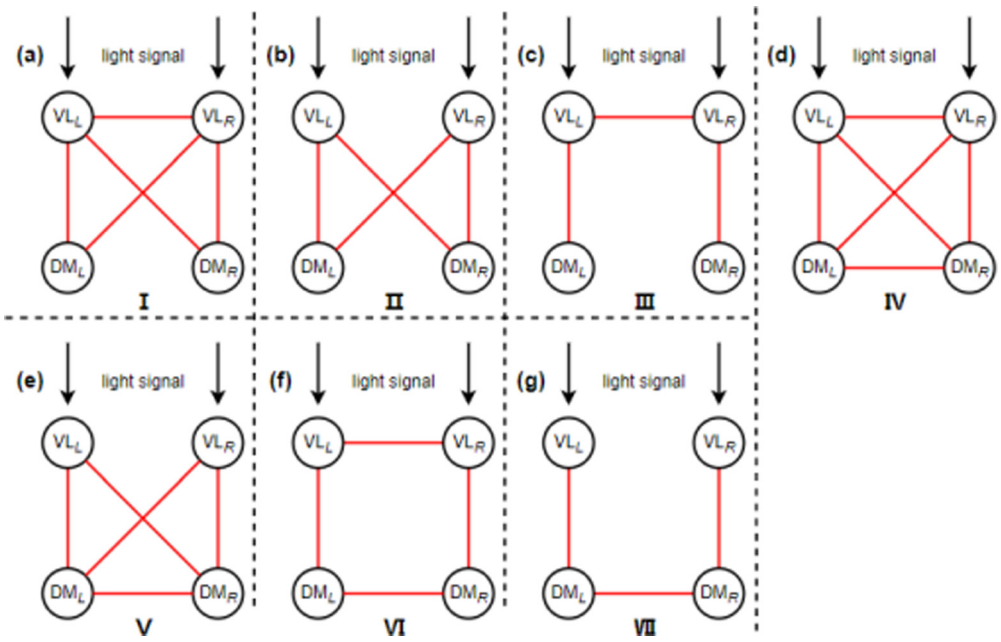

FIG. 1. Scheme of the potential motifs for the four subgroups. One circle represents one subgroup, the red line represents the connection between two subgroups, and the black line represents the light signal. Subscripts "R" and "L" represent the right nucleus of the SCN and the left nucleus of the SCN, respectively. Note that this figure does not show the details of the connections between neurons within each subgroup.

of differential equations:

$$\begin{aligned}
\dot{x}_i &= \gamma x_i(A - r_i) - \frac{2y_i\pi}{\tau} + gF_i + L_iK_f \sin\Omega_e t,\\
\dot{y}_i &= \gamma y_i(A - r_i) + \frac{2x_i\pi}{\tau}, \quad i = 1, 2, \ldots, N,\\
F_i &= \frac{1}{p_i}\sum_{j=1}^{N} e_{ij}x_j,\\
p_i &= \sum_{j=1}^{N} e_{ij}, \qquad (1)
\end{aligned}$$

where i represents the i_{th} neuronal oscillator. The parameter γ represents the relaxation parameter of a single oscillator, and the parameters A and τ represent the intrinsic amplitude and intrinsic period of the individual oscillator, respectively. The neuronal oscillators are coupled through the local field term gF_i, where g represents the coupling strength between neurons, and the value of F_i depends on the mean value of the output variable x from i's neighbors. p_i is the degree of node i, which is equal to the number of i's neighbors.

The parameter r_i is the amplitude of the i_{th} neuronal oscillator, which reads

$$r_i = \sqrt{x_i^2 + y_i^2}, \quad i = 1, 2, \ldots, N. \qquad (2)$$

$L_iK_f \sin\Omega_e t$ represents the term of light, which is determined by the location of the neurons. The parameters K_f, Ω_e, and t represent the light sensitivity, the angular frequency of the external light-dark cycle, and external time. Under constant darkness conditions, there is no difference between the VL and the DM in this model. Exposed to an external light-dark cycle, the difference between the VL and the DM is that the VL neuronal oscillators receive the light signal and relay it to the DM neuronal oscillators. If the neuronal oscillator i is located in the VL, then the parameter $L_i = 1$; and if the neuronal oscillator i is located in the DM subgroup, then the parameter $L_i = 0$.

C. Definition of the LLE

In the following sections, we will investigate the effect of the motif structure on the entrainment range of the SCN network. Here, the entrainment range can be represented by the lower limit of entrainment (LLE) [3]. The LLE is defined as the shortest T cycle that the SCN can entrain and synchronize to, and the difference from 24 h is a representation for the entrainment range of the SCN. The smaller the value of the LLE is, the broader the entrainment range is, and vice versa. The entrainment of the SCN to the external light-dark cycle is determined by the difference between the external periods T_e, where $T_e = \frac{2\pi}{\Omega_e}$, and the period T_i of each SCN neuronal oscillator. If this difference is small, meaning that $\sqrt{\frac{1}{N}\sum_{i=1}^{N}(T_i - T_e)^2} < \delta$, where δ is selected as 0.00001 h, then the SCN is considered to be synchronized or entrained to the external cycle [3]. The period of each neuronal oscillator T_i is calculated based on the evolution of y_i.

To avoid the effect of the endogenous period τ_D of the SCN on the LLE, we defined the normalized LLE as the reference [3],

$$\text{LLE}_{\text{normalized}} = \frac{\text{LLE}}{\tau_D} \times 24. \qquad (3)$$

For simplicity, the LLE represents $\text{LLE}_{\text{normalized}}$ throughout the article.

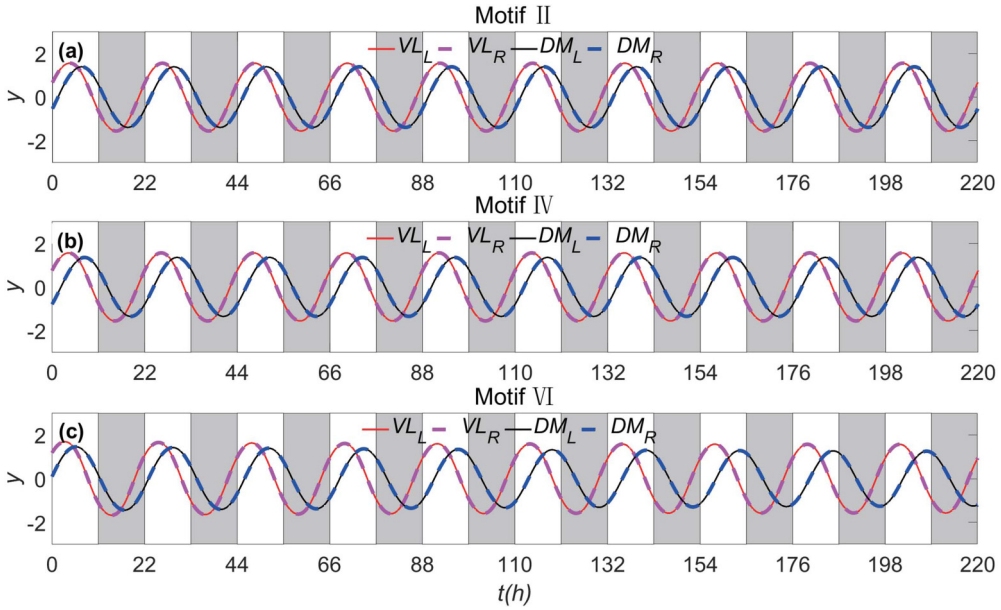

FIG. 2. Temporal evolutions of each subgroup in selected motifs exposed to the external cycles of $T_e = 22$. The gray regions correspond to darkness and the white regions correspond to light. The light sensitivity is $K_f = 0.20$, and the number of SCN neuron oscillators is $N = 4$.

D. Simulation details

As in Ref. [3], the parameters are set as $A = 1$, $g = 0.1$, and $\tau = 24$. The relaxation rates $\gamma = 0.1$, 0.2, 0.5, or 1.0 are considered, respectively. Because it is unknown if the light sensitivity is larger than the coupling strength or not, the value of K_f is selected from 0 to 0.2. In the numerical simulations, the number of neurons N was set as 200, i.e., each subgroup contained 50 oscillators. To examine the effect of the number of neuronal oscillators, we have also selected the number of neurons $N = 4$ for numerical simulations, i.e., each subgroup contained 1 oscillator, and we found that the results of $N = 4$ were similar to the results of $N = 200$.

We used the fourth-order Runge-Kutta method for the numerical simulations with time steps of 0.01 h. To avoid the effect of transients, the initial 1 000 000 time steps (10 000 h) were neglected. In the model, the initial conditions of the variables x_i and y_i are randomly selected from a uniform distribution in the range from 0 to 1.

III. NUMERICAL RESULTS

Figure 2 illustratively shows the differential influence of the motif structure on the entrainment of the SCN exposed to an artificial 22 h light-dark cycle. For Motif II in Fig. 2(a) and Motif IV in Fig. 2(b), the SCN is entrained to the external 22 h cycle, because the phase difference between (neurons in) each subgroup and the external cycle is fixed. For Motif VI in Fig. 2(c), the VL parts in both nuclei are entrained to the external cycle, but the DM parts are not, since the phase difference between the (neurons in the) DM parts and the external cycle is not fixed as they have a longer period than 22 h. Accordingly, the whole SCN network is not entrained to the external cycle in Fig. 2(c). This shows that the motif structure affects the entrainment of the SCN.

Next, it is shown how the motif structure affects the relationship between the LLE and the light sensitivity K_f in Fig. 3 for the four relaxation rates $\gamma = 0.1$, 0.2, 0.5, and 1.0 in Figs. 3(a)–3(d). For all motif connection patterns we observe a similar positive relationship between the entrainment range and K_f. In particular, when K_f is 0, which corresponds to the constant dark condition, the value of LLE is the same as the endogenous 24 h period of the SCN for each motif. If the sensitivity to light increases, then the LLE decreases, and as such the entrainment range increases. At a certain critical

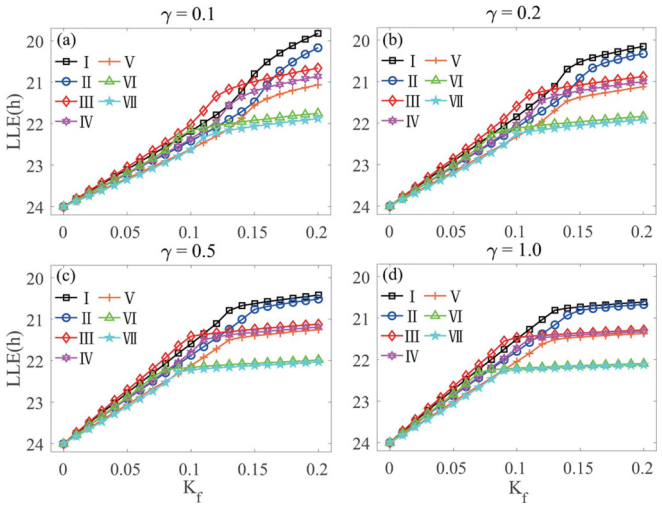

FIG. 3. A comparison in the relationships of the LLE to the light sensitivity K_f among the seven motif structures. Four relaxation parameters are considered, γ =0.1, 0.2, 0.5 and 1 in (a–d), respectively. The number of SCN neuronal oscillators is $N = 200$. Note that the positive relationship between the entrainment range and the K_f corresponds to the negative relationship between the LLE and the K_f.

value of K_f, the LLE plateaus does not decrease further. This means that the maximal entrainment range has been reached. Higher light influence will not lead to an entrained condition of the SCN outside this range. This plateau is more apparent for higher relaxation rates.

We now compare the entrainment range (represented by the LLE) among the seven motifs in Fig. 3. If K_f is a small value close to 0, smaller than the critical value, then the order of the motif connection patterns going from the smallest to the largest LLE (the largest to the smallest entrainment range) is motifs III, I, VI, IV, II, VII, and V. If the plateau values corresponding to maximum entrainment ranges, i.e., where the K_f is a large value close to 0.2, then the order of the motif connection patterns from smallest to largest LLE is motifs I, II, III, IV, V, VI, and VII. The seven network motifs can be roughly divided into three groups, among which the entrainment ranges of motifs I and II are the largest, followed by motifs III, IV, and V, and the entrainment ranges of motifs VI and VII are the smallest. By comparing the seven motifs, we find that when the two VL subgroups are coupled and the VL in one nucleus is coupled with the DM in the other nucleus, the maximum entrainment range can be obtained. When only the two DM subgroups are coupled, the minimum entrainment range can be obtained. Comparing motifs II and III, it can be seen that the coupling of the VL and the DM across different nuclei leads to a larger entrainment range than the coupling of the VL subgroups. Comparing motifs I and IV, it can be seen that the coupling of the two DM subgroups reduces the entrainment range. This indicates that the presence of a link between the VL_R and the VL_L widens the entrainment range of the SCN, whereas in the presence of a link between the DM_R and the DM_L, the entrainment range of the SCN narrows.

Analyzing similar motif connection patterns more closely, we find that the appearance of connections between both the VL_R and the VL_L and between the DM_R and the DM_L lead to entrainment ranges that are between both extremes. For example, motifs III, VI and VII are similar connection patterns, where motif III has the highest entrainment range and motif VII has the lowest entrainment range, while motif VI is in between. Also, motifs I, IV, and V show the same result.

We further investigated whether the effect of the different motif connection patterns is affected by the number of the SCN neuronal oscillators N. When the number is $N = 4$, each neuronal oscillator now represents one subgroup. The results are shown in Fig. 4 and these are consistent with the shown in Fig. 3. Therefore, the number of oscillators does not influence the effect of the motif connection patterns.

Experimental results show that the intrinsic neuronal periods differ between the VL and the DM, i.e., the DM runs faster than the VL [56]. To examine whether the differences in the intrinsic periods affect the results, the intrinsic periods of neuronal oscillators in the VL and the DM regions is set as $\tau = 24.5$ h and $\tau = 23.5$ h, respectively. The results shown in Fig. 5 are consistent with Fig. 3.

Experimental evidence shows that the number of neurons in each subgroup of the SCN was unequal, in which the VL is composed of about 25% SCN neurons and the DM is composed of about 75% SCN neurons [12]. To examine whether the proportion of the VL and the DM neurons in the SCN has

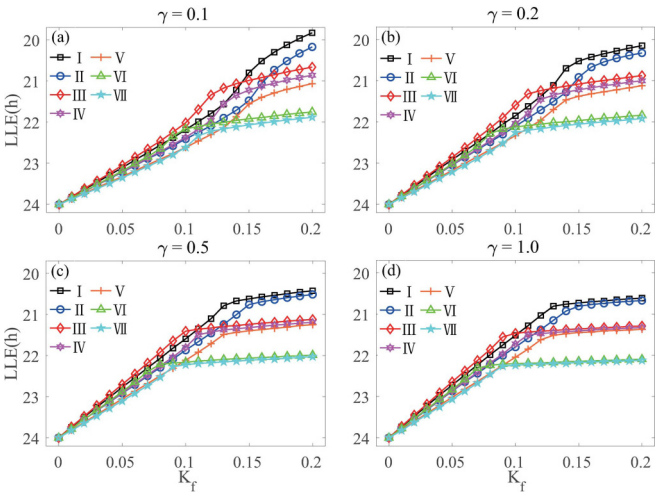

FIG. 4. A comparison in the relationship between the LLE and the light sensitivity K_f among the seven motif structures when the number of SCN neuron oscillators is $N = 4$. The values of other parameters are the same as Fig. 3.

an impact on the results, when the number of oscillators is selected as $N = 200$, where the number of the VL neurons in each nuclei are 25 and the number of the DM neurons in each nuclei are 75. The numerical simulation results show that when the light sensitivity is relatively large, Figs. 6 and 3 are qualitatively consistent, and the symmetry breaking of the numbers does not affect the results obtained.

IV. ANALYTICAL RESULTS

For simplicity, we consider the case of $N = 4$. Since the VL (or the DM) of the left nucleus and the VL (or the DM) of the right nucleus are symmetric in each motif, these two VL parts can be represented by one oscillator a, and these two

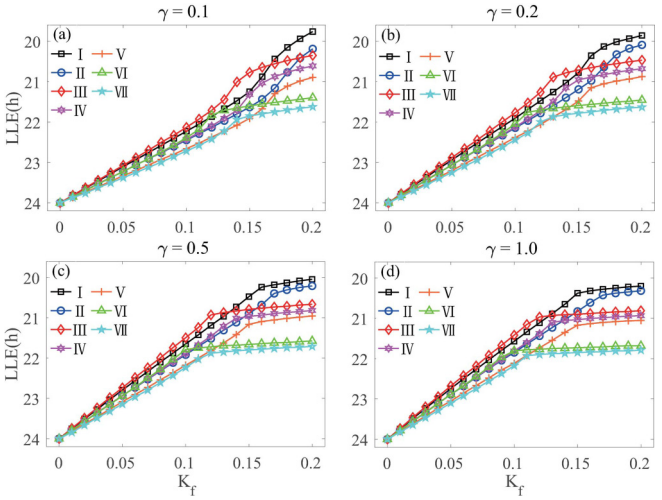

FIG. 5. A comparison in the relationship between the LLE and the light sensitivity K_f among the seven motif structures when the intrinsic periods are 24.5 h for the VL neurons and 23.5 h for the DM neurons. The number of SCN neuronal oscillators is $N = 4$. The values of other parameters are the same as Fig. 3.

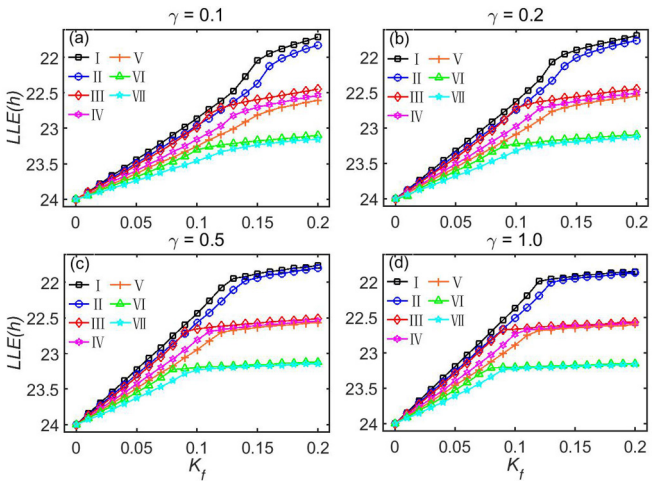

FIG. 6. A comparison in the relationship of the LLE to the light sensitivity K_f among the seven motif structures. The number of SCN neuron oscillators is $N = 200$, where neuron number of the VL in each nuclei is 25 and the neuron number of the DM in each nuclei is 75. The values of other parameters are the same as Fig. 3.

DM parts can be represented by one oscillator b. Therefore, the motif composed of four nodes can be described by the Poincaré model as follows:

$$\begin{aligned}
\dot{x}_a &= \gamma x_a(A - r_a) - \omega y_a + gF_{\mathrm{VL}} + K_f \sin \Omega_e t,\\
\dot{y}_a &= \gamma y_a(A - r_a) + \omega x_a,\\
\dot{x}_b &= \gamma x_b(A - r_b) - \omega y_b + gF_{\mathrm{DM}},\\
\dot{y}_b &= \gamma y_b(A - r_b) + \omega x_b,
\end{aligned} \tag{4}$$

where $\omega = \frac{2\pi}{\tau}$ and $\Omega_e = \frac{2\pi}{T_e}$. $F_{\mathrm{VL}} = \frac{(m_1+1)x_a + nx_b}{m_1+1+n}$ and $F_{\mathrm{DM}} = \frac{nx_a+(m_2+1)x_b}{n+m_2+1}$ represent the mean-field F of the VL subgroup and the DM subgroup, respectively, where "1" represents the self link of the neuron. m_1 represents the number of links between the two VL parts across nuclei; m_2 represents the number of links between the two DM parts across nuclei; n represents the number of links between the VL and the DM across nuclei or within the same nucleus. The values of m_1, m_2, and n are shown in Table I for Figs. 1(a)–1(g).

For convenience, we transform Eq. (4) from Cartesian coordinates to polar coordinates. Let $x_a = r_a \cos\theta_a$, $y_a = r_a \sin\theta_a$, $x_b = r_b \cos\theta_b$, $y_b = r_b \sin\theta_b$, $\phi_a = \theta_a - \Omega t$, and $\phi_b = \theta_b - \Omega t$. After substitute them into Eq. (4), we obtain

$$\begin{aligned}
\dot{r}_a = {}& \gamma r_a(A - r_a) + \frac{(m_1+1)gr_a}{m_1+1+n}\cos^2(\phi_a + \Omega t)\\
&+ \frac{ngr_b}{m_1+1+n}\cos(\phi_b + \Omega t)\cos(\phi_a + \Omega t)\\
&+ K_f \sin\Omega t \cos(\phi_a + \Omega t),
\end{aligned}$$

TABLE I. The values of m_1, m_2, and n for Figs. 1(a)–1(g).

	I	II	III	IV	V	VI	VII
m_1	1	0	1	1	0	1	0
m_2	0	0	0	1	1	1	1
n	2	2	1	2	2	1	1

$$\begin{aligned}
\dot{\phi}_a = {}& \omega - \frac{(m_1+1)g}{m_1+1+n}\cos(\phi_a + \Omega t)\sin(\phi_a + \Omega t)\\
&- \frac{ngr_b}{(m_1+1+n)r_a}\cos(\phi_b + \Omega t)\sin(\phi_a + \Omega t)\\
&- \frac{K_f}{r_a}\sin\Omega t \sin(\phi_a + \Omega t),\\
\dot{r}_b = {}& \gamma r_b(A - r_b) + \frac{ngr_a\cos(\phi_a + \Omega t)\cos(\phi_b + \Omega t)}{n+m_2+1}\\
&+ \frac{(m_2+1)gr_b}{n+m_2+1}\cos^2(\phi_b + \Omega t),\\
\dot{\phi}_b = {}& \omega - \frac{ngr_a}{(n+m_2+1)r_b}\cos(\phi_a + \Omega t)\sin(\phi_b + \Omega t)\\
&- \frac{(m_2+1)g}{n+m_2+1}\cos(\phi_b + \Omega t)\sin(\phi_b + \Omega t).
\end{aligned} \tag{5}$$

Considering the averaging method developed by Krylov and Bogoliubov as used in Refs. [3,46,48,57,58], ϕ has a lower timescale than Ωt. Letting $\alpha = \langle\phi_a\rangle - \langle\phi_b\rangle$, we get

$$\begin{aligned}
\langle\cos^2(\phi_a + \Omega t)\rangle &= \frac{1}{2},\\
\langle\cos(\phi_b + \Omega t)\cos(\phi_a + \Omega t)\rangle &= \frac{\cos\alpha}{2},\\
\langle\cos(\phi_a + \Omega t)\sin(\phi_a + \Omega t)\rangle &= 0,\\
\langle\cos(\phi_b + \Omega t)\sin(\phi_a + \Omega t)\rangle &= \frac{\sin\alpha}{2},\\
\langle\sin(\Omega t)\cos(\phi_a + \Omega t)\rangle &= -\frac{\langle\sin\phi_a\rangle}{2},\\
\langle\sin(\Omega t)\sin(\phi_b + \Omega t)\rangle &= \frac{\langle\cos\phi_b\rangle}{2},
\end{aligned} \tag{6}$$

where $\langle\cdot\rangle$ denotes the average in one light-dark cycle. For simplicity, we keep the nonaveraged notation r_a, r_b, ϕ_a, and ϕ_b in the following. When the SCN neuronal oscillator is entrained to the light-dark cycle, $\dot{r}_a = 0$, $\dot{r}_b = 0$, $\dot{\theta}_a = 0$, and $\dot{\theta}_b = 0$ are obtained. Substituting Eq. (6) into Eq. (5), we obtain Eq. (7):

$$\begin{aligned}
0 = {}& \gamma r_a(A - r_a) + \frac{g[(m_1+1)r_a + nr_b\cos\alpha]}{2(m_1+1+n)}\\
&- \frac{K_f}{2}\sin\phi_a,\\
\Omega = {}& \omega - \frac{nr_b}{2(m_1+1+n)r_a}g\sin\alpha - \frac{K_f}{2r_a}\cos\phi_a,\\
0 = {}& \gamma r_b(A - r_b) + \frac{g[nr_a\cos\alpha + (m_2+1)r_b]}{2(n+m_2+1)},\\
\Omega = {}& \omega + \frac{nr_a}{2(n+m_2+1)r_b}g\sin\alpha.
\end{aligned} \tag{7}$$

Intuitively, when Ω achieves the maximal value, i.e., $\mathrm{LLE} = \frac{2\pi}{\Omega_{\max}}$. In the following, we will show the effect of the motif structure on $\Omega_{\max}$ under two extreme conditions, i.e., K_f is close to 0 and K_f is close to 0.2, respectively.

When K_f is close to 0, we simulate the phase information versus time for each motif, as shown in Fig. 7. It can be seen that $\sin\alpha \approx \alpha$ and $\cos\theta_a \approx -1$, so we obtain $\cos\alpha \approx 1$.

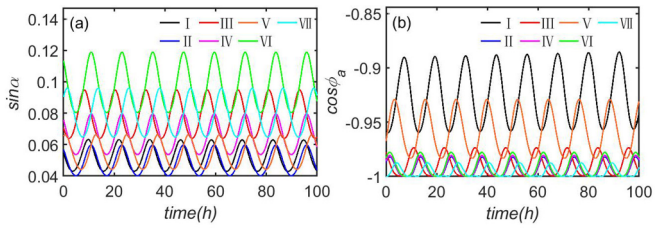

FIG. 7. Under the LLE, the phase information for $N = 4$ neuronal oscillators. (a) The phase difference between the VL and the DM in the sine form for each motif, (b) the phase difference between the VL and the light-dark cycle in the cosine form for each motif. The coupling strength is $g = 0.1$, and the light sensitivity is $K_f = 0.01$. This figure shows numerical simulations based on Eq. (1).

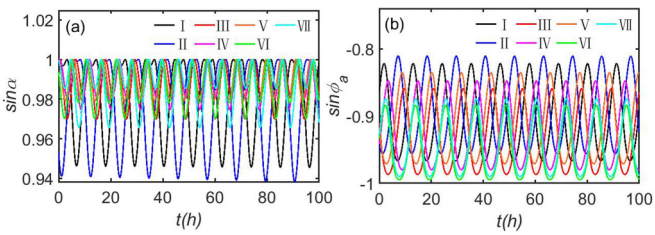

FIG. 8. Under the LLE, the phase information for $N = 4$ neuronal oscillators. (a) The phase difference between the VL and the DM in the sine form for each motif, (b) the product of the phase difference in the sine form between the VL and the light-dark cycle for each motif. The coupling strength is $g = 0.1$, and the light sensitivity is $K_f = 0.20$.

Therefore, Eq. (7) can be simplified as

$$\begin{aligned} 0 &= \gamma r_a(A - r_a) + \frac{g[(m_1+1)r_a + nr_b]}{2(m_1+1+n)} \\ &\quad - \frac{K_f}{2}\sin\phi_a, \\ \Omega &= \omega - \frac{nr_b}{2(m_1+1+n)r_a}g\alpha + \frac{K_f}{2r_a}, \\ 0 &= \gamma r_b(A - r_b) + \frac{g[nr_a + (m_2+1)r_b]}{2(n+m_2+1)}, \\ \Omega &= \omega + \frac{nr_a}{2(n+m_2+1)r_b}g\alpha. \end{aligned} \tag{8}$$

When $K_f \to 0$, the effect of the light sensitivity is very small, thus, $r_a \approx r_b$. Due to $\sin\phi_a \approx 0$, we obtain

$$r_a \approx A + \frac{g}{2\gamma}. \tag{9}$$

From the second equation and the last equation of Eq. (8), we obtain

$$\begin{aligned} \Omega &= \omega - \frac{nr_b}{4(m_1+1+n)r_a}g\alpha \\ &\quad + \frac{nr_a}{4(n+m_2+1)r_b}g\alpha + \frac{K_f}{4r_a} \\ &= \omega + \left(\frac{n}{n+m_2+1} - \frac{n}{m_1+1+n}\right)\frac{g\alpha}{4} \\ &\quad + \frac{K_f}{4(A+\frac{g}{2\gamma})}. \end{aligned} \tag{10}$$

For structures I and III,

$$\frac{n}{n+m_2+1} - \frac{n}{m_1+1+n} = \frac{1}{6}. \tag{11}$$

For structures II, IV, and VI,

$$\frac{n}{n+m_2+1} - \frac{n}{m_1+1+n} = 0. \tag{12}$$

For structures V and VII,

$$\frac{n}{n+m_2+1} - \frac{n}{m_1+1+n} = -\frac{1}{6}. \tag{13}$$

We obtain $\Omega_{\max}$ of structures II, IV, and VI, which is smaller than structures I and III and larger than structures V and VII. Therefore, we confirm the numerical finding for the left side of Fig. 3.

Moreover, we examine the case of K_f close to 0.2. The phase information versus time for each motif, as shown in Fig. 8, and it can be seen that $\sin\alpha \approx 1$. Thus, Eq. (7) can be simplified as

$$\begin{aligned} 0 &= \gamma r_a(A - r_a) + \frac{g[(m_1+1)r_a + nr_b\cos\alpha]}{2(m_1+1+n)} \\ &\quad - \frac{K_f}{2}\sin\phi_a, \\ \Omega &= \omega - \frac{nr_b}{2(m_1+1+n)r_a}g - \frac{K_f}{2r_a}\cos\phi_a, \\ 0 &= \gamma r_b(A - r_b) + \frac{g[nr_a\cos\alpha + (m_2+1)r_b]}{2(n+m_2+1)}, \\ \Omega &= \omega + \frac{nr_a}{2(n+m_2+1)r_b}g. \end{aligned} \tag{14}$$

Because $\cos\phi_a$ is close to -1, and the change of the second equation of Eq. (14) is much larger than the fourth equation, the LLE is determined by the fourth equation. Thus, we obtain

$$\Omega = \omega + \frac{nr_a}{2(n+m_2+1)r_b}g. \tag{15}$$

Because the influence of $\frac{r_a}{r_b}g$ is very small, Eq. (15) can be approximated by

$$\Omega = \omega + \frac{n}{2(n+m_2+1)}g. \tag{16}$$

For structures I and II,

$$\begin{aligned} \Omega_{\max}(I) > \Omega_{\max}(II) &\approx \omega + \frac{n}{2(n+m_2+1)} \\ &= \omega + \frac{1}{3}. \end{aligned} \tag{17}$$

For structures III, IV, and V,

$$\begin{aligned} &\Omega_{\max}(III) > \Omega_{\max}(IV) > \Omega_{\max}(V) \\ &\approx \omega + \frac{n}{2(n+m_2+1)} \\ &= \omega + \frac{1}{4}. \end{aligned} \tag{18}$$

For structures VI and VII,

$$\Omega_{\max}(VI) > \Omega_{\max}(VII) \approx \omega + \frac{n}{2(n+m_2+1)} = \omega + \frac{1}{6}. \quad (19)$$

Because $\mathrm{LLE} = \frac{2\pi}{\Omega_{\max}}$, a smaller LLE corresponds to a larger $\Omega_{\max}$, that is, a larger entrainment range. From the above analysis, we can get that structures I and II show strong entrainment, structures III, IV, and V show medium entrainment, and structures VI and VII show weak entrainment. This analytical result is qualitatively consistent with the numerical simulation results in Fig. 3.

V. CONCLUSION AND DISCUSSION

Thus far, the communications between the VL and the DM have only been inspected within one nucleus and the cross-communication between the left and the right nucleus was not taken into account. Previous research has shown that there is communication present between these two nuclei, although its precise mechanism has not been precisely known yet [22]. Enhancing knowledge about how connection patterns between the VL and the DM of both the left and the right nucleus influence the synchronization and entrainment ability of the SCN as a whole helps to understand how the interplay between the left and the right nucleus can be utilized by the SCN network to create stable and robust rhythms in ever-changing environmental conditions.

In this article, we theoretically analyzed seven motiflike connection patterns to investigate the network of the two nuclei of the SCN as a whole, with each nucleus containing two subgroups of neurons, one that is sensitive to light (the VL subgroup) and one that is insensitive to light (the DM subgroup). Using the motif structures as a basis provided us with information on the topology of the network of the two nuclei of the SCN, and we connected this to the entrainment property of the SCN.

The main finding was that the coupling between the VL subgroups, the cross coupling between the VL subgroup and the DM subgroup are more conducive to the increase of the entrainment range, and the latter has more influence than the former, while the coupling between the DM subgroups decreases the entrainment range and has the greatest influence on the entrainment range.

Changing the strengths of the connections between the different regions (VL and DM) of the two SCN nuclei may be utilized by the SCN to accomodate changes in external conditions, such as resynchronization after a jet lag, adjustment to photoperiod or for the aging SCN. This mechanism may be used in future treatments that improve health and well-being of the elderly.

ACKNOWLEDGMENTS

This work is supported by the National Natural Science Foundation of China under Grant No. 11875042 (C.-G. Gu), Natural Science Foundation of Shanghai under Grant No. 21ZR1443900 (C.-G. Gu), and the Shanghai project for construction of top disciplines under Grant No. USST-SYS01 (H.-J. Yang and C.-G. Gu).

[1] C. S. Pittendrigh, Annu. Rev. Physiol. **55**, 17 (1993).
[2] R. Refinetti, *Circadian Physiology* (CRC Press, Boca Raton, FL, 2006).
[3] U. Abraham *et al.*, Mol. Syst. Biol. **6**, 438 (2010).
[4] C. S. Pittendrigh and S. Daan, J. Comp. Physiol. A **106**, 223 (1976).
[5] J. Aschoff and H. Pohl, Naturwissenschaften **65**, 80 (1978).
[6] J. H. Meijer, B. Rusak, and M. E. Harrington, Brain Res. **501**, 315 (1989).
[7] S. Michel and J. H. Meijer, Eur. J. Neurosci. **51**, 482 (2020).
[8] M. Sujino, S. Koinuma, Y. Minami, and Y. Shigeyoshi, J. Biol. Rhythms **36**, 410 (2021).
[9] J. H. Meijer and W. J. Schwartz, J. Biol. Rhythms **18**, 235 (2003).
[10] H. S. Lee, J. L. Nelms, M. Nguyen, R. Silver, and M. N. Lehman, Nat. Neurosci. **6**, 111 (2003).
[11] H. T. VanderLeest, J. H. T. Rohling, S. Michel, and J. H. Meijer, PLoS ONE **4**, e4976 (2009).
[12] J. H. T. Rohling, H. T. VanderLeest, S. Michel, M. J. Vansteensel, and J. H. Meijer, PLoS ONE **6**, e25437 (2011).
[13] C. Gu, Z. Liu, W. J. Schwartz, and P. Indic, PLoS ONE **7**, e36900 (2012).
[14] S. M. Reppert and D. R. Weaver, Annu. Rev. Physiol. **63**, 647 (2001).
[15] D. Gonze, S. Bernard, C. Waltermann, A. Kramer, and H. Herzel, Biophys. J. **89**, 120 (2005).
[16] C. G. Gu, J. S. Xu, J. Rohling, H. J. Yang, and Z. H. Liu, PLoS ONE **10**, e0145360 (2015).
[17] C. G. Gu, P. Wang, T. Weng, H. J. Yang, and J. H. T. Rohling, Math. Biosci. Eng. **16**, 1893 (2019)
[18] M. Nagano, K. Ikegami, Y. Minami, Y. Kanazawa, S. Koinuma, M. Sujino, and Y. Shigeyoshi, Brain Res. **1714**, 73 (2019).
[19] T. L. Leise, A. Goldberg, J. Michael, G. Montoya, S. Solow, P. Molyneux, R. Vetrivelan, and M. E. Harrington, Eur. J. Neurosci. **51**, 2343 (2020).
[20] H. O. de la Iglesia *et al.*, Curr. Biol. **14**, 796 (2004).
[21] C. Gu, H. Yang, and J. H. T. Rohling, Phy. Rev. E **95**, 032302 (2017).
[22] S. Michel *et al.*, Eur. J. Neurosci. **37**, 964 (2013).
[23] J. H. Abel *et al.*, Proc. Natl. Acad. Sci. USA **113**, 4512 (2016).
[24] R. Silver and W. J. Schwartz, Methods Enzymol. **393**, 451 (2005).
[25] S. J. Aton, C. S. Colwell, A. J. Harmar, J. Waschek, and E. D. Herzog, Nat. Neurosci. **8**, 476 (2005).
[26] L. P. Morin, J. Biol. Rhythms **22**, 3 (2007).
[27] V. Reghunandanan and R. Reghunandanan, J. Circadian Rhythms **4**, 2 (2006).
[28] H. E. Albers, J. C. Walton, K. L. Gamble, J. K. McNeill, and D. L. Hummer, Front. Neurol. **44**, 35 (2017).

[29] C. Vasalou, E. D. Herzog, and M. A. Henson, J. Biol. Rhythms. **24**, 243 (2009).
[30] T. L. To, M. A. Henson, E. D. Herzog, and F. J. Doyle, Biophys. J. **92**, 3792 (2007).
[31] D. DeWoskin *et al.*, Proc. Natl. Acad. Sci. USA **112**, E3911 (2015).
[32] R. Milo, S. Shen-Orr, S. Itzkovitz, N. Kashtan, D. Chklovskii *et al.*, Science **298**, 824 (2002).
[33] R. Milo, S. Itzkovitz, N. Kashtan, R. Levitt, S. Shen-Orr, I. Ayzenshtat *et al.*, Science **303**, 1538 (2004).
[34] F. Battiston, V. Nicosia, M. Chavez, and V. Latora, Chaos. Interdisc. J. Nonlin. Sci. **27**, 047404 (2017).
[35] Y. Wei, X. Liao, C. Yan, Y. He, and M. Xia, Hum. Brain. Map. **38**, 2734 (2017).
[36] C. Duclos, D. Nadin, Y. Mahdid, V. Tarnal, P. Picton, G. Vanini, and S. Blain-Moraes, Sci. Rep. **11**, 3892 (2021).
[37] L. Gollo and M. Breakspear, Philos. Trans. Roy. Soc. B **369**, 20130532 (2014).
[38] L. Gollo, C. Mirasso, O. Sporns, and M. Breakspear, PLoS Comput. Biol. **10**, e1003548 (2014).
[39] O. Sporns *et al.*, PLoS Biol. **2**, e369 (2004).
[40] C. J. Honey *et al.*, Proc. Natl. Acad. Sci. USA **104**, 10240 (2007).
[41] O. Sporns, C. J. Honey *et al.*, PLoS ONE **2**, e1049 (2007).
[42] E. J. Friedman, K. Young, G. Tremper, J. Liang, A. S. Landsberg, N. Schuff, A. D. N. Initiative *et al.*, PLoS ONE **10**, e0124453 (2015).
[43] C. A. Czeisler *et al.*, Science **284**, 2177 (1999).
[44] A. Campuzano, J. Vilaplana, T. Cambras, and A. Diez-Noguera, Physiol. Behav. **63**, 171 (1998).
[45] S. Usui, Y. Takahashi, and T. Okazaki, Am. J. Physiol. Regul. Integr. Comp. Physiol. **278**, R1148 (2000).
[46] C. Gu, J. Xu, Z. Liu, and J. H. T. Rohling, Phys. Rev. E **88**, 022702 (2013).
[47] A. E. Granada, G. Bordyugov, A. Kramer, and H. Herzel, PLoS ONE **8**, e59464 (2013).
[48] C. Gu, A. Ramkisoensing, Z. Liu, J. H. Meijer, and J. H. T. Rohling, J. Biol. Rhythms **29**, 16 (2014).
[49] G. Bordyugov, U. Abraham, A. Granada, P. Rose, K. Imkeller, A. Kramer, and H. Herzel, J. R. Soc. Interface **12**, 20150282 (2015).
[50] C. Bodenstein, M. Gosak, S. Schuster, M. Marhl, and M. Perc, PLoS Comput. Biol. **8**, e1002697 (2012).
[51] C. Schmal, J. Myung, H. Herzel, and G. Bordyugov, Front. Neurol. **6**, 94 (2015).
[52] I. T. Tokuda, D. Ono, B. Ananthasubramaniam, S. Honma, K. I. Honma, and H. Herzel, Biophys. J. **109**, 2159 (2015).
[53] C. Gu, M. Tang, H. Yang, and J. H. T. Rohling, Sci. Rep. **6**, 37661 (2016).
[54] C. Gu, H. Yang, and M. Wang, Phy. Rev. E **96**, 052207 (2017).
[55] C. Gu, J. H. T. Rohling, X. M. Liang, and H. J. Yang, Phys. Rev. E **93**, 032414 (2016).
[56] T. Noguchi, K. Watanabe, A. Ogura, and S. Yamaoka, Eur. J. Neurosci. **20**, 3199 (2004).
[57] A. Balanov, N. Janson, D. Postnov, and O. Sosnovtseva, *Synchronization: From Simple to Complex* (Springer-Verlag, New York, NY, 2009).
[58] C. Gu, H. Yang, and Z. Ruan, Phys. Rev. E **95**, 042409 (2017).